Pergamon

*Int. J. Heat Mass Transfer.* Vol. 40, No. 13, pp. 3135–3147, 1997

Printed in Great Britain
0017-9310/97 $17.00+0.00

PII: S0017-9310(96)00348-1

# Enhancing forced air convection heat transfer from an array of parallel plate fins using a heat pipe

Z. ZHAO† and C. T. AVEDISIAN‡

Sibley School of Mechanical and Aerospace Engineering, Cornell University, Ithaca, NY 14853-7501, U.S.A.

(*Received* 5 *August* 1996 *and in final form* 1 *October* 1996)

**Abstract**—An experimental study of heat transfer from an array of copper plate fins supported by a copper heat pipe and cooled by forced air flow is presented. The results are compared to an identical array of copper fins, but supported by a solid copper rod. The primary variable is the height of the fin stack, while the fin pitch, air flow rate, surface area and fin shape are fixed. The results show that for some conditions fins of fixed pitch supported by a heat pipe dissipate higher heat transfer rates for the same surface temperature than fin arrays supported by a solid rod. The difference in heat transfer rates decreases as the height of the fin stack decreases. Maximum steady state heat fluxes and total powers were measured to be 80 W cm$^{-2}$ and 800 W, respectively, for the tallest fin stack studied (10.16 cm) for an approach air velocity of 5.9 m s$^{-1}$ and a surface temperature rise above the ambience of 160°C. The fin stack supported by a solid copper rod dissipated 30 W cm$^{-2}$ and 300 W for the same conditions. For the smallest height examined (2.54 cm) no significant advantage was realized by using a heat pipe to support the fin stack. A simplified analysis is also presented to predict surface temperature for a known heat input for both heat pipe supported and solid rod supported plate fin arrays. Predicted and measured values are in good agreement. © 1997 Elsevier Science Ltd.

## 1. INTRODUCTION

When fins are attached to a surface, the highest heat transfer rate will be realized if the fin base and heat source temperatures are the same. This limit is realized only for a fin base material of infinite thermal conductivity. Heat pipes can, if properly designed, approach this limit better than any known material including diamond. Effective thermal conductivities of heat pipes, that are thousands of times higher than diamond, can be realized under some conditions [1]. Heat pipes can, thus, be an effective means for bridging the thermal path between the heat source and fin base, thereby enhancing heat transfer from the fins.

This paper reports the results of a study of heat transfer from an array of parallel plate fins of fixed pitch maintained by a support rod that is either a heat pipe or solid material (see Fig. 1). The purpose is to: (1) compare the performance of a heat pipe to a solid rod for the plate fin structure schematically illustrated in Fig. 1(a); (2) examine the effect of support rod length, $H$, on the heat transfer rate; and (3) develop a simple model to predict heat transfer. The air flow velocity and fin pitch are fixed and the height $H$ of the module is variable. The plate fin array is supported by a single rod [Fig. 1(a)] which is either a heat pipe or solid (copper) rod whose purpose is to maintain the fin pitch and transport heat away from the flat base plate. The flat base plate facilitates attachment of a heater. For a support rod that is a heat pipe, the finned region serves as the condenser section.

The plate fin model shown in Fig. 1 is well suited for a heat pipe. Circular heat pipes are comparatively easy to manufacture and the technology for stacking fins around them with good thermal contact exists. However, little systematic experimentation has been reported which provides information for designing such a heat sink or predicting its performance. Chao [2] studied heat transport from a configuration similar to that shown in Fig. 1(a). Several wick structures (powder metal and integral groove), working fluids (water and methanol) and orientations were examined. Total power dissipation of up to 250 W using water was measured. The relatively large evaporator area limited heat fluxes to under 10 W cm$^{-2}$. A heat sink consisting of multiple tube (heat pipe) supports for a parallel plate array [Fig. 1(b)] was also studied [3] and heat fluxes of up to 31 W cm$^{-2}$ and total powers of 1400 W were realized using copper heat pipe supports, water for the working fluid, a sintered powder metal wick and an approach air flow velocity of 5.3 m s$^{-1}$. In another study [4], heat transfer from a plate fin array using multiple heat pipe supports was compared to an unfinned array of the same number of tubes attached to a base plate (e.g. a pin fin heat sink, in which the pins are heat pipes). Significant

†Current address: ETH Zentrum, CH-8092 Zurich, Switzerland.

‡Author to whom correspondence should be addressed.

## NOMENCLATURE

| | |
|---|---|
| $A_{cyl}$ | total area of unfinned portion of support tube |
| $Bi_D$ | $h\,2D/k$ |
| $D_{wi}$ | wick inner diameter |
| $D_{wo}$ | wick outer diameter |
| $D$ | outer diameter of support tube |
| $h_{cyl}$ | heat transfer coefficient for unfinned portion of support tube |
| $H$ | height of fin array |
| $k$ | thermal conductivity of solid support tube |
| $k_{air}$ | thermal conductivity of air |
| $k_w$ | thermal conductivity of wick |
| $L$ | length of square fin |
| $L_a$ | length of support tube end cap |
| $M$ | total number of fins in the fin array |
| $Pr$ | Prandtl number |
| $q_{in}$ | power input to base plate |
| $q_i$ | conduction heat transfer rate into $i$th element (Fig. 5). |
| $Q_i$ | $2q_i/\pi kDT_\infty$ |
| $R_{tot}$ | total thermal resistance |
| $Re_L$ | Reynolds number of air flow over fin surface, $VL/\nu$ |
| $R_{fi}$ | thermal resistance of a single annular fin |
| $T_c$ | average temperature over region of heat input in base plate |
| $T_\infty$ | ambient temperature |
| $V$ | average air velocity between fins, 5.9 m s$^{-1}$. |

Greek symbols

| | |
|---|---|
| $\delta$ | fin thickness |
| $\Delta$ | spacing between fins |
| $\psi$ | orientation angle [Fig. 1(a)] |
| $\Delta T$ | $T_c - T_\infty$ |
| $\Delta x_i$ | spacing of the $i$th element [Fig. 5] |
| $\Delta\bar{x}_i$ | $\Delta x_i/D$ |
| $\theta_i$ | $(T_i - T_\infty)/T_\infty$ |
| $\nu$ | kinematic viscosity. |

enhancements in heat transfer were realized for the finned tube array compared to the unfinned sink for air velocities up to 7 m s$^{-1}$. These studies have contributed significantly to our understanding of the performance of fin arrays supported by heat pipes. However, systematic comparisons and analyses of heat transfer from a fin structure that employs a solid rod for maintaining fin pitch to one that uses a heat pipe support have not been reported. These aspects are examined in the present study for the basic configuration of a single rod structure shown in Fig. 1(a) that is a building block to the multiple tube module [Fig. 1(b)].

A decision to use a heat pipe in a configuration like that shown in Fig. 1 is a tradeoff between the cost of using a solid material for the fin support and the potential for improved heat transfer by using a heat pipe. Heat pipes are a relatively mature technology [5–8] and are finding increasing use in many commercial products because of improvements in manufacturability which have made them cost effective and reliable [9]. For example, heat pipes are currently used in several laptop computer product lines [10].

Heat pipes may not always enhance heat transport for several reasons. Firstly, the potential for dryout, characterized by the inability of the wick to draw fluid from the condenser section back to the evaporator section at the same rate that fluid is evaporated, will limit the maximum steady state heat transfer rate. Secondly, the effective thermal conductivity of a heat pipe is dependent on the working fluid properties and wick structure and material. Thirdly, as $H$ is reduced a limit is approached where heat transport by conduction (rather an vaporization and liquid return) through the heat pipe wall, wick and vapor core can be controlling. A heat pipe would then not be as efficient for transporting energy as a solid material. Conversely, a solid support tube loses its effectiveness as $H$ increases due to the progressive drop in temperature along the tube.

## 2. EXPERIMENT

### 2.1. *Module design*

Figure 2 shows a cross-section of the design. The physical size was chosen based on a workstation cooling environment. The thermal modules consist of an array of parallel plate fins attached to a rod which maintains the fin pitch. The finned region serves as the condenser section of the heat pipe support rod. The rod is attached to a flat base plate to facilitate attachment to a heated surface. The plate fin modules shown in Fig. 2 were designed with virtually no adiabatic section to eliminate the pressure drop and associated thermal resistance. Two types of structures were fabricated: one in which the support rod and base plate were heat pipes and another in which the rod and plate were solid copper.

To promote vapor flow to the central support rod for the heat pipe modules, the base plate contained an array of holes in a spoke-like network toward the center. Each hole was lined with a wick material as schematically illustrated in Fig. 2. The expected flow pattern is shown in Fig. 2(a). Heat input into the base plate evaporates fluid in the wick. The vapor flows

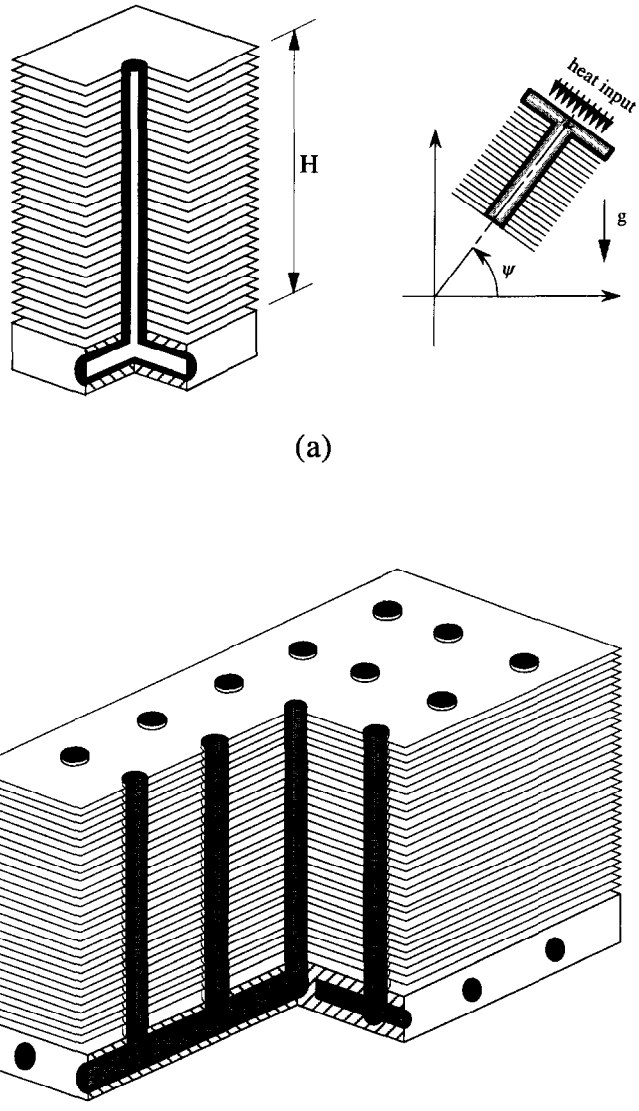


Fig. 1. Schematic diagram of parallel plate module: (a) single support rod module; (b) multiple support rod module.

toward the central hole where it enters the fin support rod and then condenses as it travels down the support rod due to heat removal by the fins attached to the rod (through forced air flow across the fin array). The condensate is drawn back to the base plate by the capillary action of the wick which lines the inner wall of the support rod, and the wick lining the holes in the base plate further distributes the condensate in a more or less uniform pattern over the heater foot print where the process is repeated.

The wick structure consisted of a sintered copper powder material that was fabricated in an operation that is proprietary to Thermacore, Inc., (Lancaster, Pa). Sintered metal powder wicks have been previously studied and shown to be effective for promoting heat transfer and liquid return to the evaporator section [11, 12]. The porosity and permeability of the wicks fabricated here is approximately 50% and $2.1 \times 10^{-7}$ cm$^2$, respectively. The effective capillary radius of curvature of the wick structure (length scale of a pore opening) is about 45 $\mu$m. The wick thickness is 1.57 mm for the condenser tube and 0.79 mm for the base plate holes. The condenser tube was brazed to the evaporator plate before the wick sintering process to ensure a continuous wick structure from the condenser tube to the base plate channels.

The fins are $50.8 \times 50.8$ mm rectangular copper plates and brazed to the support tube with 14 fins per 2.54 cm yielding a fin spacing $\Delta$ of approximately 1.43 mm. Modules were filled with the working fluid (water) by a steam–blow process. Water was first

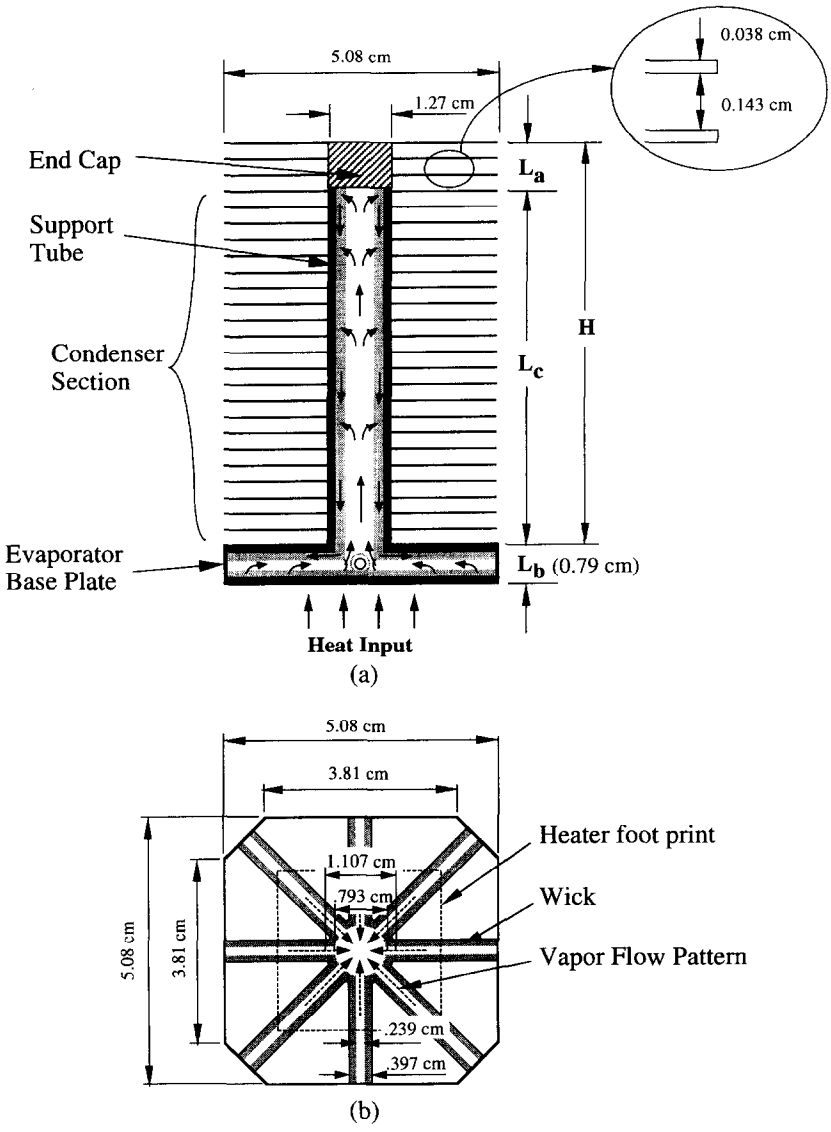


Fig. 2. Detail of parallel plate module showing cross-section of heat pipe support with vapor flow patterns.

injected into an evacuated module through a hole at the end of the support tube to fill approximately 70% of the void volume of the sintered copper wick. The chamber was then heated to between 100 and 105°C to evaporate approximately 20% of the water, after which the chamber was sealed. A 0.813 mm thick copper disk cap was brazed to the end of the heat pipe and sealed with a stycast epoxy rod of the same diameter as the condenser tube [length $L_a$ in Fig. 2(a)]. The thickness of the brazed layer is 0.076 mm and the height of the stycast epoxy rod is 6.35 mm.

To examine the influence of varying $H$ [Fig. 2(a)] on heat transport and to compare a heat pipe module with a solid module, a total of eight plate fin modules of the design shown in Fig. 1(a) were fabricated: four of the heat pipe modules [Fig. 2(a)] and four comprised entirely of solid copper with identical outer dimensions. The module heights were 25.4, 50.8, 76.2 and 101.6 mm.

### 2.2. *Test facility*

To create controlled conditions for forced air flow through the finned modules, the wind tunnel shown in Fig. 3 was constructed. It was designed so that each module completely filled the tunnel cross-section. Because $H$ was variable, the tunnel had a moveable wall with various inserts to provide a smooth transition to accommodate the range of $H$ examined. For convenience only the top wall of the wind tunnel was moveable. This design created some asymmetry in the velocity profile (slightly higher velocity near the moveable wall), which was reduced somewhat by placing test modules 12 cm downstream of the transition insert. An array of screens and flow straighteners were placed upstream of the insert to improve the uniformity of the flow entering the diverging section.

Measurements were made of the surface temperature and power to the base plate while holding

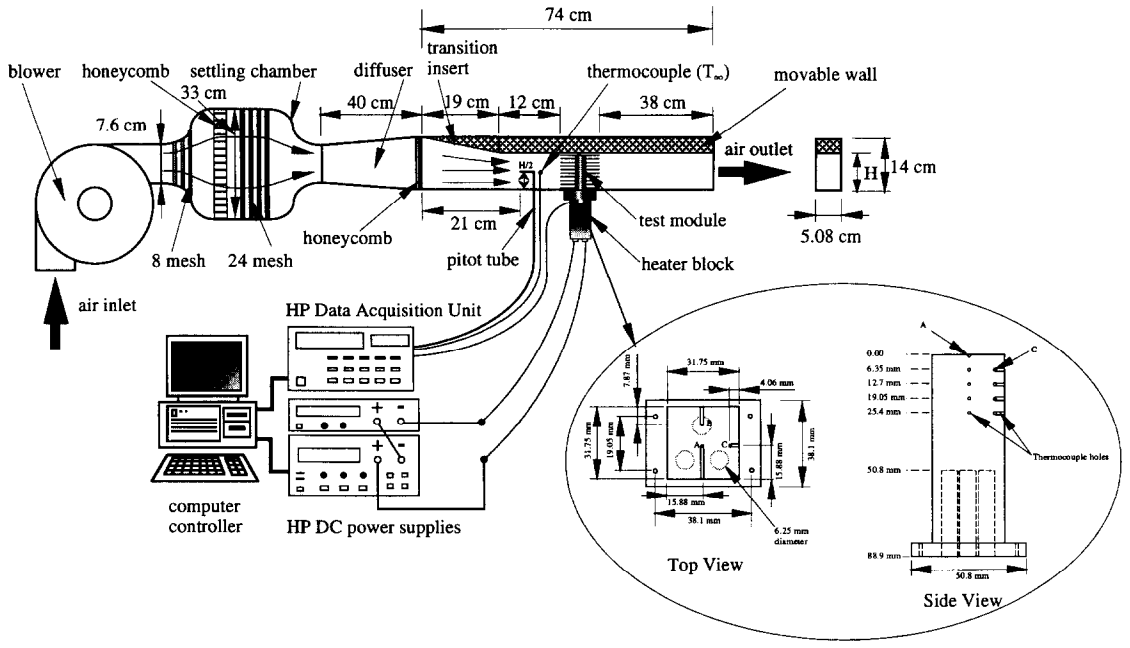


Fig. 3. Schematic diagram of wind tunnel test facility.

the air velocity upstream of the module constant. Heat input was provided by a copper block containing three cartridge heaters and several K-type (0.508 mm diameter) thermocouples as shown in the inset to Fig. 3. A thermally conductive paste was applied to the polished surface to reduce the contact resistance. At location "A" shown in Fig. 3 the uppermost thermocouple was mounted in a groove to provide a measure of the surface temperature.

Power was increased in 10 W increments and steady state conditions were reached before changing the power. At each steady state power setting, temperatures and air velocities were recorded. A period of 30 min was allowed to elapse before changing the power. This time was sufficient for steady conditions to be reached for all power values. Power was increased until limitations on temperature of the heater block (250°C) or dryout was reached.

Figure 4 illustrates a typical evolution of surface temperature difference ($\Delta T \equiv T_c - T_\infty$) for $H = 7.62$ cm and $\psi = 90°$. The data were obtained at intervals of 28.8 s for a series of power increments using a computerized data acquisition system (HP-3852A 20 channel multiplexer connected to a PC) which recorded all temperatures and controlled the input power (a typical experimental run such as shown in Fig. 4 lasted between 24 and 48 h). The symbols "A", "B" and "C" refer to conditions that will be referenced in Section 4. At "A", the module is operating in a steady condition. At "B", the first evidence of dryout is noted while between "B" and "C" a sudden excursion of temperature that signifies dryout is realized. At "C", the power increase is reduced in equal increments of 10 W. A power is eventually reached at which the temperature suddenly drops. This drop is believed to be due to re-wetting of the wick in the base plate.

The thermocouples were calibrated using a HP 2804A quartz thermometer which is accurate to $\pm 0.01$°C. The calibration was conducted at three temperatures: room temperature, 0°C using an ice bath and the saturation temperature of water (steam). The maximum difference in temperature between the thermocouples and the quartz thermometer was 0.6°C over the range 0.01°C (ice) to 99.39°C (steam).

The air velocity in the tunnel was measured with a 3.05 mm diameter pitot probe placed 10 cm upstream to the entrance of the fin array. The probe was mounted on a traverse to allow velocity measurements over the cross-section of the wind tunnel. Velocity was measured at the center of a grid consisting of 1.27 by 1.27 cm square "cells" across the channel. For the test modules with $H = 2.54$ cm, measurements were made over eight locations and for $H = 10.16$ cm measurements were made over 32 cells. The velocity varied by a maximum of 24% over the cells due to the asymmetric insert. During an experimental run, the blower was manually adjusted to maintain the air velocity at the center location of the channel ($H/2$) at 5.9 m s$^{-1}$ for all power increments and module heights, $H$.

The surface temperature, $T_c$ and the input power ($q_{in}$) into the base plate were obtained from the measured temperature gradient in the heater block rather than from the electrical power input. Linear regression of the temperatures at locations A, B and C in Fig. 3 was used to obtain the temperature gradient, and extrapolation to the surface resulted in a value of $T_c$. The temperature and the heat flux at the contact surface were determined by averaging extrapolated

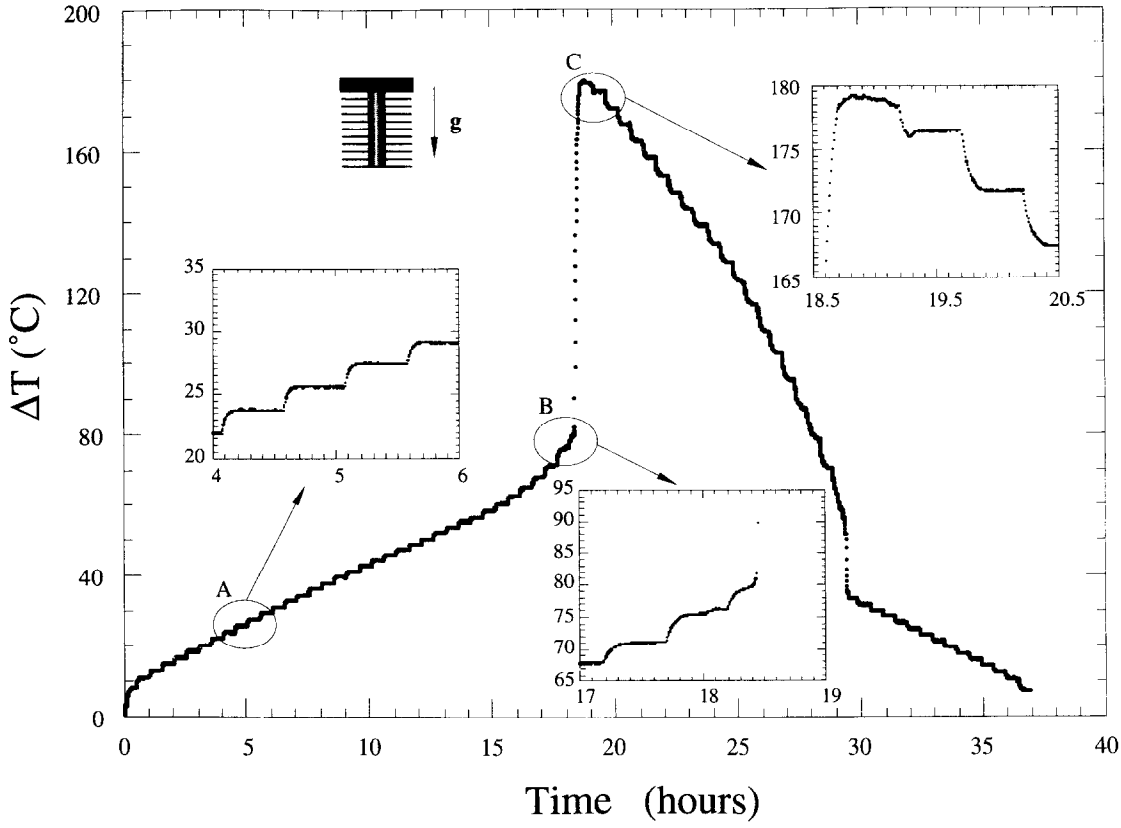


Fig. 4. Evolution of $\Delta T$ during a typical experiment for the $H = 7.62$ cm heat pipe module operating against gravity. Dryout is revealed by the temperature excursion, B→C. Insets more clearly show the effect of a step change in input power on $\Delta T$.

temperatures and heat fluxes for locations A, B and C at $x = 0$. The heat fluxes determined in this way differed from the heat input based on the electrical power input to the cartridge heaters by less than 5%, with the difference being a measure of heat loss through the insulation. Only input powers based on the measured temperature gradient are presented here.

## 3. ANALYSIS

### 3.1. *Introduction*

A simplified model is formulated based on idealized operation of a heat pipe as isothermal and heat transfer in a solid rod support as one-dimensional. This approach ignores internal transport processes such as evaporation of liquid in the wick, vapor flow to the condenser section and liquid return to the evaporator which can lead to a prediction for dryout [13]. However, general trends predicted by this approach are consistent with the experimental results, and reasonable agreement is shown with measurements as discussed in Section 4. Figure 5 shows the two models for heat transfer.

### 3.2. *Heat pipe module*

In view of the assumption being made that the heat pipe support is an isothermal rod, a simplified thermal resistance network [14] is a useful alternative to more detailed analysis of the internal liquid and vapor transport processes within the heat pipe. The ability of such a simplified approach to accurately predict heat transfer rates also depends on estimates of the various thermal resistances involved.

Figure 5 shows the resistance model. The total thermal resistance between the base plate surface at temperature $T_c$ and the ambiance at temperature $T_\infty$, $R_{tot}$, is the sum of two contributions, one due to heat spreading in the base plate ($R_b$) and the other due to the fin array:

$$R_{tot} = R_b + \left[ \frac{R_{end}\left(R_p + R_w + \dfrac{R_{cyl}R_{fin}}{R_{cyl}+R_{fin}}\right)}{R_{end} + \left(R_p + R_w + \dfrac{R_{cyl}R_{fin}}{R_{cyl}+R_{fin}}\right)} \right] \quad (1)$$

where the term in brackets is the effective thermal resistance of the plate fin array including the heat pipe support rod and unfinned portion of the rod. The overall heat transfer rate is given as

$$q_{in} = (T_c - T_\infty)/R_{tot}. \quad (2)$$

We now discuss each of the resistances in equation (1).

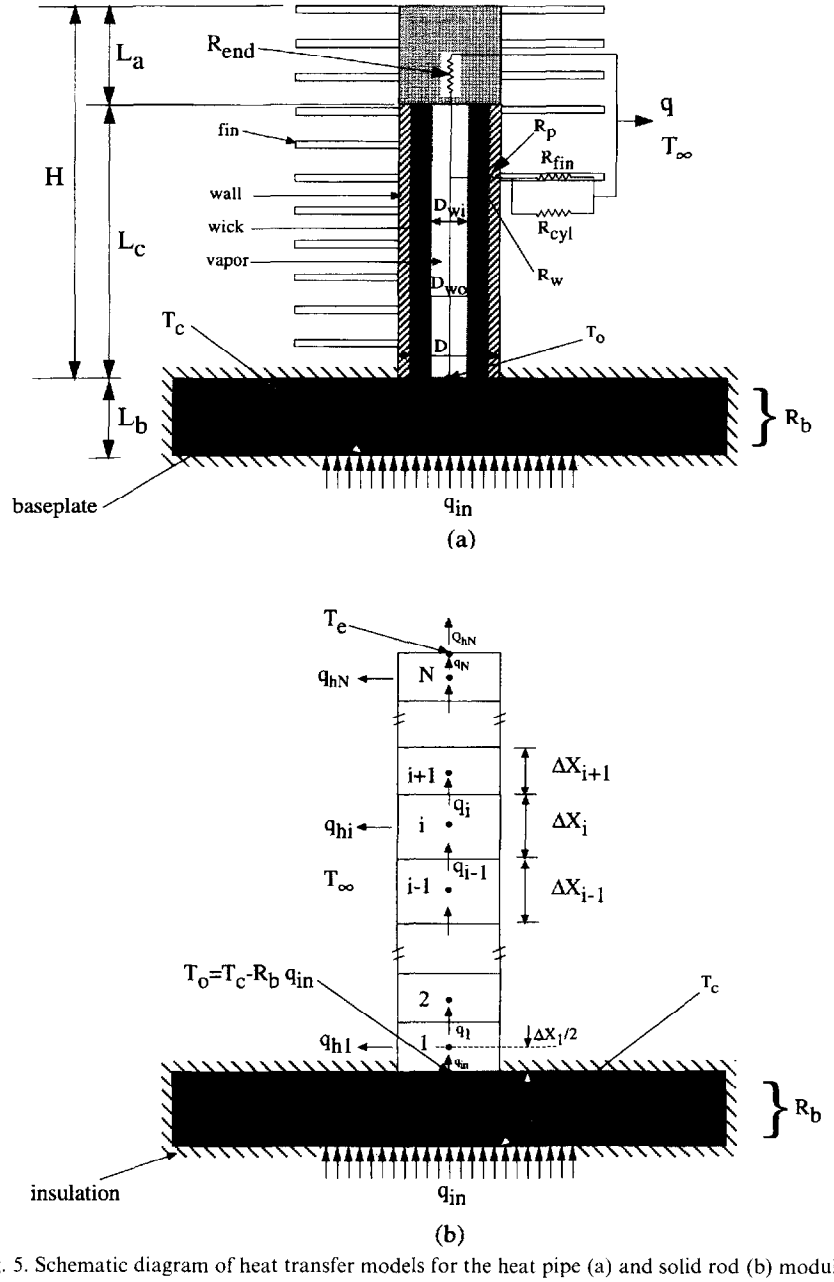


Fig. 5. Schematic diagram of heat transfer models for the heat pipe (a) and solid rod (b) modules.

The thermal resistance of the unfinned portion of the support tube, $R_{cyl}$, is approximated as

$$R_{cyl} = \frac{1}{h_{cyl} A_{cyl}} \tag{3a}$$

where

$$A_{cyl} = M\pi D(H/M - \delta) \tag{3b}$$

and $M = H/(\delta + \Delta)$ for a fixed fin pitch. The total thermal resistance of the fins, $R_{fin}$, is related to the thermal resistance of a single fin, $R_{fi}$, as $R_{fin} = R_{fi}/M$. $R_{fi}$ was evaluated by using an expression for an annular fin [15]. The heat transfer coefficients required to determine $R_{cyl}$ and $R_{fi}$ depend on the flow patterns involved. For the unfinned portion of the support tube, a standard correlation for the Nusselt number $Nu_{cyl}(\equiv h_{cyl}D/k_{air})$ for cross flow past a cylinder was used [15]:

$$Nu_{cyl} = 0.193\, Re_D^{0.618} Pr^{1/3}. \tag{4a}$$

The characteristic velocity, $V$, used in determining the Reynolds number was based on the measured centerline velocity at $H/2$ ($\approx 5.9$ m s$^{-1}$). For the surface of the plate fins, $h_{fin}$ needed to determine $R_{fi}$ was evaluated by using an expression for the Nusselt number ($Nu_{fin} \equiv h_{fin}D_e/k_{air}$) for developing flow between isothermal parallel plates [16]:

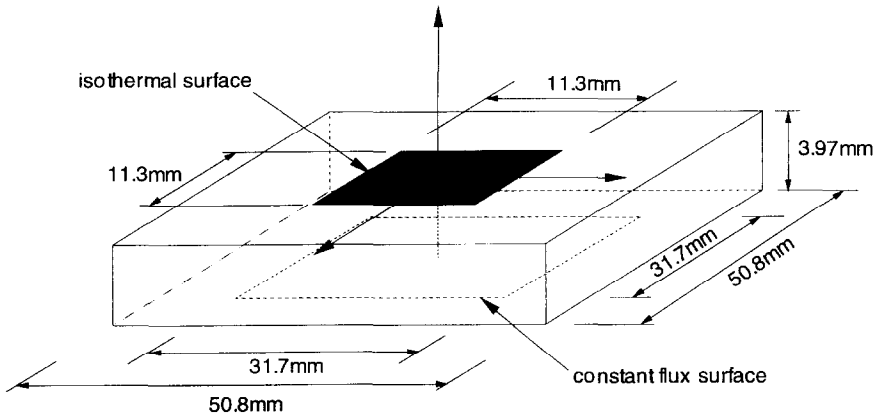


Fig. 6. Geometry for numerically determining $R_b$.

$$Nu_{fin} = 7.55 + \frac{0.024\chi^{-1.14}}{1. + 0.0358\chi^{-0.64}Pr^{0.17}} \quad (4b)$$

where $\chi \equiv x/D_e/(Re_{De} \cdot Pr)$ and $D_e = 2\Delta$ for the parallel plate fins.

$R_{end}$ was determined by assuming that conduction heat transfer in the end cap was one-dimensional and the approach described in Section 3.2 was then used. $R_w$ and $R_p$ in Fig. 5 were based on a composite cylinder as

$$R_w = \ln(D_{wo}/D_{wi})/(2\pi\{H - L_a\}k_w) \quad (5a)$$

and

$$R_p = \ln(D/D_{wo})/(2\pi\{H - L_a\}k_w. \quad (5b)$$

The wick thermal conductivity ($k_w$) in equation (5) was estimated for a sintered material using a formulation given by Peterson and Fletcher [12].

Finally, the thermal resistance of the base plate, $R_b$, resembles a two-dimensional heat spreader with specified temperature at one end and a uniform heat flux at the other [17]. No analytical solution exists for the three-dimensional configuration of interest here in which heat is input over a portion of one end of the plate and a uniform temperature patch exists over the other as shown in Fig. 6. Holes in the base plate [Fig. 2(b)] further complicate the determination of $R_b$. A conservative estimate of $R_b$ was to neglect the presence of the holes, whose function is primarily to promote vapor flow to the central support tube and then to determine $R_b$ numerically for a solid copper plate. The code FLOTHERM (Flomerics, Inc.) was applied to the quarter plane symmetry in Fig. 6 using $39 \times 21 \times 39$ cells with the result that $R_b \approx .0701$ C/W. For the solid module (see Section 3.4) this value of $R_b$ was found to be almost an order of magnitude less than $R_{tot}$ for the four values of $H$ examined, while for the shortest length examined (2.54 cm) it was small compared to the term in brackets in equation (1). $R_b$ was comparable to the bracketed term for the longest support tube (10.16 cm). The extent of agreement demonstrated in Section 4 between predicted and measured powers suggests that the uncertainties associated with estimating $h_{fin}$, $h_{cyl}$ and $R_b$ may compensate to some extent when using equation (4).

### 3.3. *Dryout*

The simple model for heat transport discussed in Section 3.2 cannot predict dryout because internal vapor and liquid transport are not considered. There are five mechanisms that can lead to dryout: those due to viscous, sonic, entertainment, boiling or capillary mechanisms. Formulations developed by Chi [5] and Busse [18] were used to obtain estimates of these limits. Comparisons with measured steady state power levels showed that the capillary limit was within the range of measured powers. The other limits were larger than the imposed heat fluxes in the experiments.

The formulation for the capillary limit [5] was applied to the modules shown in Fig. 2. The dryout heat flux was estimated by assuming that the dynamic contact angle was 0 as suggested by Chi [5] and Peterson [6] and results are shown in Section 4.

### 3.4. *Solid module*

Heat transfer through a solid rod support was modeled as one-dimensional in the axial direction. The temperature drop along the rod was obtained by a simple numerical analysis based on an energy balance on a discretized rod shown in Fig. 5(b). An energy balance for the $i$th element ($1 < i < N$) gives

$$Q_{i-1} = Q_{hi} + Q_i \quad (6)$$

where

$$Q_i = \frac{\theta_i - \theta_{i-1}}{\Delta\bar{x}_i + \Delta\bar{x}_{i+1}} \quad (7)$$

and

$$Q_{hi} = \xi_i\theta_i. \quad (8)$$

When a fin is attached to an element, then

$$\xi_i = \frac{1}{\bar{R}_{fi}} \quad (9a)$$

where $\bar{R}_{fi} = R_{fi}k\pi D/2$. When an element is bare, then

$$\xi_i = Bi_D \Delta \bar{x}_i. \tag{9b}$$

When $i = 1$ in equation (6), then

$$Q_o = Q_{in} \tag{10a}$$

$$\theta_c = \theta_o + \frac{q_{in} R_b}{T_\infty}, \tag{10b}$$

$\xi_1 = Bi_D \Delta \bar{x}_1$ and $R_b \approx .0701$°C/W as discussed in Section 3.2.

When $i = N$, then

$$Q_N = \frac{\theta_N - \theta_e}{\Delta \bar{x}_N} \tag{11a}$$

$$\theta_e = \frac{\theta_N}{\frac{Bi_D}{4} \Delta \bar{x}_N + 1} \tag{11b}$$

and $\xi_N = (1/\bar{R}_{fi})$ since a fin is always flush with the end of the support rod for the modules fabricated. The heat transfer coefficient at the tip of the rod is assumed to be the same as the average heat transfer coefficient over the fin surface ($h_{fin}$ from equation 4(b)).

Equations (6)–(11) are a tridiagonal system of algebraic equations for $\theta_i$. They were solved by the Thomas algorithm [19]. The number of elements "$i$" between each fin (separated by the distance $\Delta$) was varied from 1 to 11 and no difference in the results was found for $i \geqslant 2$. For all calculations reported here, $i = 4$ was used.

## 4. DISCUSSION OF RESULTS

Figures 7 and 8 show the variation of steady state heat flux (W cm$^{-2}$) and power ($W$) with temperature difference, $\Delta T$. Data from several runs are given to show the repeatability of the results. The approach air velocity is 5.9 m s$^{-1}$ for all of the data shown. Figure 7 shows that for gravity assisted operation, the heat pipe plate fin modules for $H = 10.16$ cm can dissipate powers approaching 600 W and heat fluxes approaching 60 W cm$^{-2}$ for $\Delta T < 100$°C which is most relevant to electronic packaging applications. For $\Delta T < 180$°C which is the largest temperature rise examined to avoid damage and oxidation of the heater block, steady state powers and fluxes approaching 800 W and 80 W cm$^{-2}$, respectively, were measured for the $H = 10.16$ cm heat pipe modules. For operation against gravity (Fig. 8), the steady state results are nearly the same as for gravity assisted operation (Fig. 7) with the exception of a dryout-like effect being revealed as shown in Figs. 8(c) and (d). That orientation does not affect steady state performance in the pre-dryout regime shows the dominance of forced

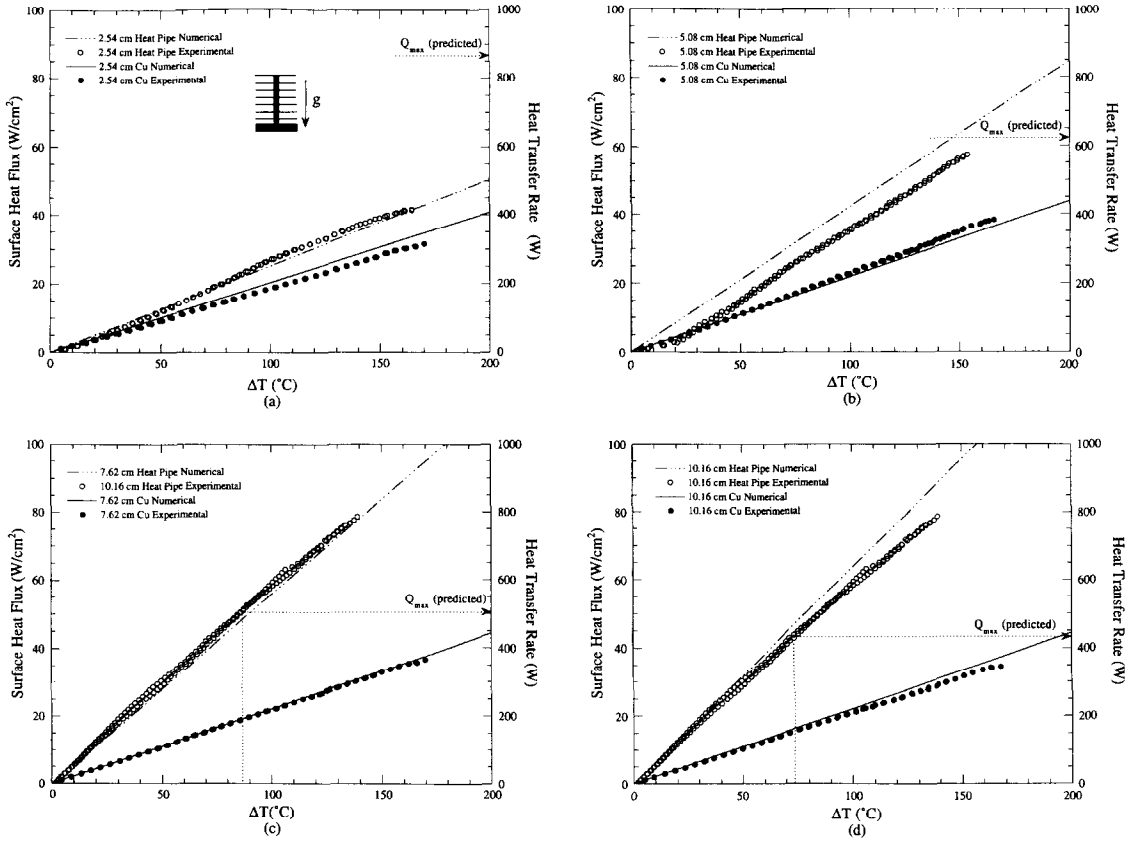


Fig. 7. Variation of steady state heat flux and power with $\Delta T$ for the parallel plate modules operated with gravity assistance.

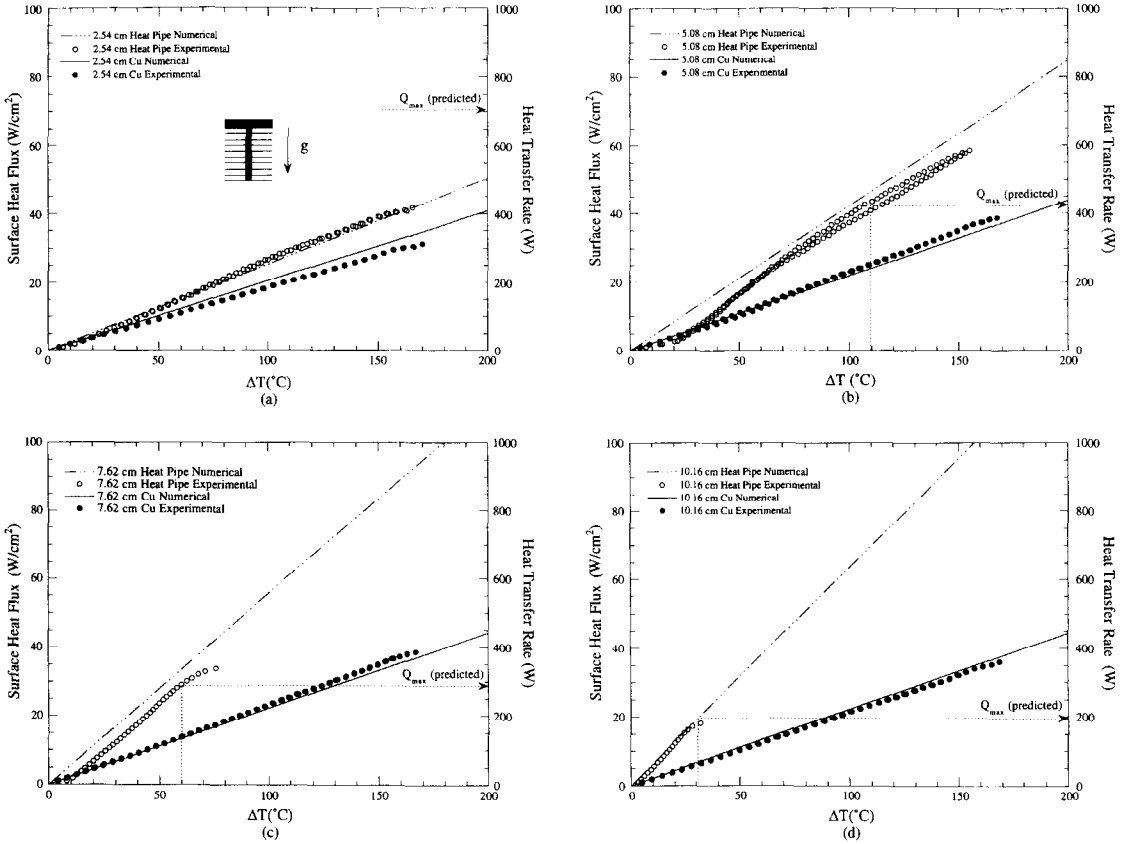


Fig. 8. Variation of steady state heat flux and power with $\Delta T$ for the parallel plate modules operated against gravity.

convection in the fin stack and the strong capillary pumping ability of the sintered wick structure.

The lines shown in Figs. 7 and 8 are predictions from the analysis. Agreement between measured and predicted powers and heat fluxes is good considering the approximations involved in the analysis of Section 3. The accuracy of the predicted values is dependent in part on the heat transfer coefficients ($h_{\text{fin}}, h_{\text{cyl}}$), the choice of a characteristic velocity for the Reynolds number, and the thermal resistance of the base plate ($R_b$). As mentioned previously, the centerline velocity at $H/2$ in Fig. 3, 5.9 m s$^{-1}$, was used for the characteristic velocity for the calculation of Reynolds number. A sensitivity analysis was done to determine the influence of uncertainties in $h_{\text{fin}}$, $V$, and $R_b$ on the predictions. A range of velocity of $\pm 12\%$ (to correspond to the 24% variation over the flow cross-section) resulted in a change of $h_{\text{cyl}}$ and $h_{\text{fin}}$ by about 10%. An uncertainty of 10% for $h_{\text{fin}}$ and $h_{\text{cyl}}$ using equation (4) resulted in a maximum change of 5% in predicted power levels from the values given in Figs. 7 and 8 for the shortest height examined ($H = 25.4$ mm); the changes were smaller as $H$ increased. The results were less sensitive to variations in $R_b$. Variations of 10% in $R_b$ from the value of 0.0701°C/W determined numerically for a solid copper base plate (Fig. 6) resulted in less than a 2% change in predicted power.

To understand the qualitative trends shown in Figs. 7 and 8, a simple model of the plate fin module is used which assumes the heat pipe support rod is isothermal such that the base of each plate fin is at the contact temperature, $T_c$ and that all heat is dissipated through the fins. For the solid rod support, the temperature drop along the rod is accounted for by using a fin analysis of the support rod to estimate the base temperature for each plate fin. For illustration purposes only, we neglect the contribution of the unfinned portion of the support tube (the model of Section 3 includes this effect) and assume $\Delta \gg \delta$. For the heat pipe support

$$q_{\text{in}} = \xi \Delta T H/\Delta \tag{12a}$$

and for the solid support rod module

$$q_{\text{in}} = \xi \Delta T[f_\Delta + f_{2\Delta} + \cdots + f_H] \tag{12b}$$

where

$$\xi \equiv \pi k D \delta \sqrt{\frac{2h_{\text{fin}}}{k\delta}}\,\lambda \tag{12c}$$

(for an annular fin $\lambda$ is a function of $h_{\text{fin}}$, $D$, $k$ and $\delta$ [15]). The function $f_\Delta$ depends on the boundary conditions assumed for the support rod "fin". For example, an insulated end boundary condition gives $f_\Delta = \cosh(\zeta\{H-\Delta\})/\cosh(\zeta H)$ where $\zeta \equiv 2\sqrt{h_{\text{cyl}}/kD}$

and for a "long" fin $f_\Delta = e^{-\zeta\Delta}$. For typical boundary conditions of fins, $f_H$ is independent of $H$ as $H \to \infty$ so that in this limit $q_{in}$ also becomes independent of $H$ from equation (12b). We now discuss the trends in Figs. 7 and 8 for fixed parameters (e.g. $\Delta$, $\xi$ and $\zeta$) and variable $H$ and $\Delta T$.

An isothermal support rod for which a heat pipe support rod is a limit would result in $\partial q_{in}/\partial \Delta T$ being proportional to $H$ from equation (12a). This limit appears to be closely approached for the modules examined as shown in Figs. 7 and 8 where it is seen that doubling the support rod length nearly doubles the power for given $\Delta T$, a result which can only arise if the support rod is isothermal. For a solid rod support, however, Figs. 7 and 8 show essentially no dependence on $H$ which is consistent with equation (12b) and the analysis of Section 3.4 for $H$ large enough that $f_H$ is independent of $H$ in equation (12b).

For the heat pipe support, a value of $\Delta T$ appears to be reached above which $\partial q_{in}/\partial \Delta T$ noticeably decreases. This result could arise if (the comparatively high thermal conductivity) liquid in the base plate is replaced by (the lower thermal conductivity) vapor due to a dryout mechanism. The identification of dryout based on a decrease in $\partial q_{in}/\partial \Delta T$ is consistent with sintered metal powder wick structures [11]. The effect is considerably more noticeable when $\psi = 90°$ than when $\psi = -90°$ since in the former case the capillary action of the wick alone is responsible for liquid return to the base plate while in the latter case gravity aids liquid return.

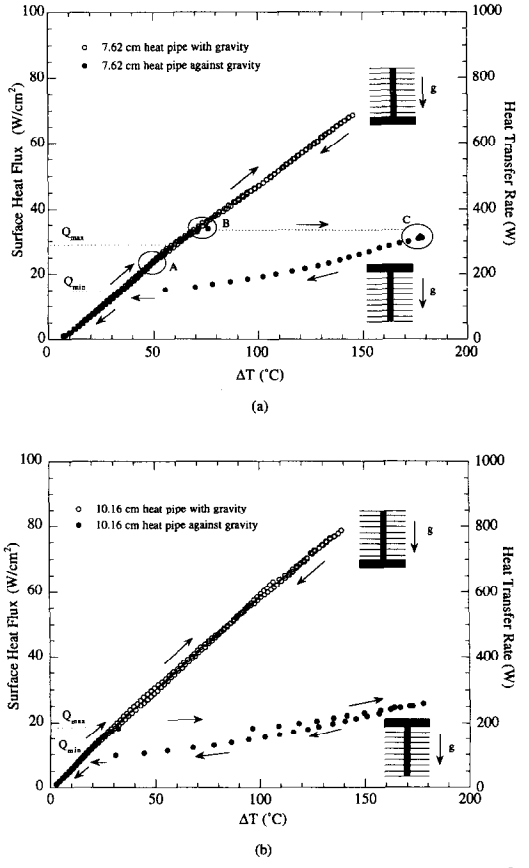


Fig. 9. Variation of heat flux and power input with $\Delta T$ for $H = 7.62$ mm (a) and $H = 10.16$ mm (b). Dryout is revealed for operation against gravity (Figs. 7 and 8 show only predryout data).

Shown in Figs. 7 and 8 are predicted values of the dryout heat flux ($Q_{max}$) from the capillary limit formulation presented by Chi [5]. Values ranged from 431 to 865 W for the four finned modules studied when $\psi = -90°$ and 197 to 709 W for $\psi = 90°$. These values are higher than measured steady state powers for $\psi = -90°$ where no evidence for dryout (signified by a decrease in $\partial q_{in}/\partial \Delta T$) was observed for this orientation.

To further illustrate dryout, Fig. 9 shows typical variations of surface heat flux with $\Delta T$ in greater detail for the two orientations for the $H = 7.62$ cm and 10.16 cm heat pipe support tubes. (Only data up to but not including the dryout and post dryout region are shown in Figs. 7 and 8.) The arrows indicate the direction in which the power was changed. The symbols "A", "B" and "C" in Fig. 9 are referenced to Fig. 4. As shown in Fig. 9, dryout was not noticeable for gravity assisted operation, ($\psi = -90°$) for both values of $H$. However for $\psi = 90°$, a clear reduction of $\partial q_{in}/\partial \Delta T$ is observed for $\Delta T > 70°C$ when $H = 7.62$ cm and for $\Delta T > 30°C$ when $H = 10.16$ cm. The variation of surface temperature with power follows two tracts in the post-dryout regime, which is typical of a "hysteresis" effect in boiling that arises due to variations in the dynamic contact angle associated with the onset of dryout and then re-wetting.

Typical variations of $\Delta T$ with $H$ for two representative power levels is shown in Fig. 10 for $\psi = -90°$ [Figs. 10(a) and (b)] and $\psi = 90°$ [Figs. 10(c) and (d)], respectively. The solid lines are predictions from the model, and the agreement is reasonable. For the solid rod support, $\Delta T$ is almost independent of $H$ for $H > 30$ mm which is consistent with equation (12b) when $H > 30$ mm. For the heat pipe support, however, $\Delta T$ depends strongly on $H$ for given power input for all values of $H$ examined, which is consistent with equation (12a) where $\Delta T \propto 1/H$ for given $q_{in}$.

## 5. CONCLUSIONS

Five major conclusions are the following:

(1) Heat transfer from an array of parallel plate fins in forced air flow can be significantly increased by using a heat pipe to maintain fin pitch.

(2) A simplified model based on an isothermal support rod for a heat pipe and a one-dimensional temperature distribution in a solid rod was shown to predict reasonably well the measured power dissipation for given surface temperature and upstream air velocity. Though dryout can-

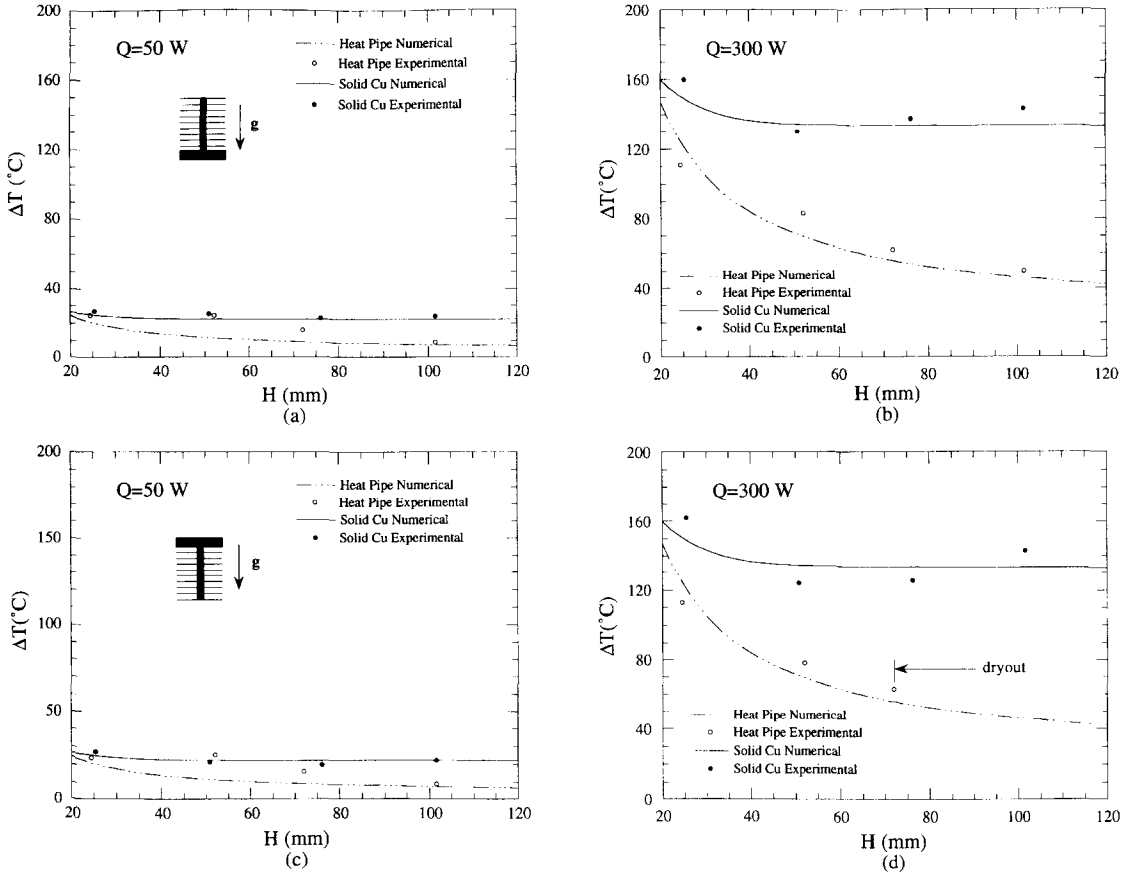


Fig. 10. Variation of $\Delta T$ with $H$ for two input powers (50 W and 300 W) and orientations.

not be predicted by the model, the experimental results suggest that the capillary limit is likely the most relevant one for the modules examined for restricting the maximum heat flux.

(3) The parallel plate fin modules were very effective for dissipating high powers and fluxes at moderate surface temperatures. For temperatures most relevant to electronic cooling applications ($<100^{\circ}$C), total powers of over 400 W and 40 W cm$^{-2}$ were measured for the heat pipe modules fabricated. For higher surface temperatures, up to 150°C, steady state powers of 800 W and 80 W cm$^{-2}$ were measured depending on orientation.

(4) The heat transport rate is proportional to the module height for the heat pipe modules, which is a reflection of their nearly isothermal operation. For the solid copper rod support, the heat transfer rate was nearly independent of module height. This result is due to the fact that the end of the solid copper support rod was already close to the ambient temperature for the shortest module height examined.

(5) Differences in the heat transfer rate between the heat pipe modules and solid copper modules were substantial for the tallest modules examined (10.16 cm). For the shortest modules examined (2.54 cm), using a heat pipe support to maintain fin pitch offered little advantage over a solid rod support.

*Acknowledgements*—The authors acknowledge the many helpful discussions throughout the course of this study with Mr Brian Fritsch of Thermacore, Inc., Drs Roger Schmidt, Sanjeev Sathe, Bahgat Sammakia and Gregory Chrysler of IBM, and Professor Che-Yu Li of Cornell. Thanks are also due to Messrs Robert deHoff and Jerry Toth of Thermacore for their technical expertise in the design and fabrication of the heat pipes. This study was supported by the Semiconductor Research Corporation (Dr Ron Bracken, monitor) and the Industry-Cornell Alliance for Electronic Packaging (Dr Che-Yu Li, monitor).

## REFERENCES

1. Silverstein, C. C., Effective thermal conductivity of heat pipes. AIAA paper no. 94-1962, 1994.
2. Chao, S., Thermal management of high-power TAB IC chips incorporating heat spreaders and heat pipes. *Proceedings of 9th International Heat Transfer Conference*, Vol. 2, 1990, pp. 295–300.
3. North, M. T. and Avedisian, C. T., Heat pipes for cooling high flux/high power semiconductor chips. *Journal of Electronic Package*, 1993, **115**, 112–117.
4. Howard, A. H. and Peterson, G. P., Investigation of a heat pipe array for convective cooling, HTD—Vol. 278. *Fundamentals of Heat Pipes*. 1994, ASME, New York, pp. 11–19.

5. Chi, S. W., *Heat Pipe Theory and Practice: A Sourcebook*. Hemisphere Publishing Co., Washington, 1976.
6. Peterson, G. P., *An Introduction to Heat Pipes*. Wiley, New York, 1994.
7. Dunn, P. D. and Reay, D. A., *Heat Pipes*, 4th edn. Pergamon Press, New York, 1994.
8. Faghri, A., *Heat Pipe Science and Technology*. Taylor and Frances, 1995.
9. Waller, L., An old idea may solve VHSIC cooling problem. *Electronics*, 1985, pp. 19–20.
10. Schmidt, R. C., Personal Communication, July 10, 1995.
11. Pruzan, D. A., Klingensmith, L. K., Torrance, K. E. and Avedisian, C. T., Design of high performance sintered wick heat pipes. *International Journal of Heat and Mass Transfer*, 1991, **34,** 1417–1427.
12. Peterson, G. P. and Fletcher, L. S., Effective thermal conductivity of sintered heat pipe wicks. *Journal of Thermophysics and Heat Transfer*, 1987, **1,** 343–347.
13. Pruzan, D. A., Torrance, K. E. and Avedisian, C. T., Two-phase flow and dryout in a screen wick saturated with a fluid mixture. *International Journal of Heat and Mass Transfer*, 1990, **33,** 673–681.
14. Asselman, G. A. A. and Green, D. B., Heat pipes: I. Operation and characteristics. *Philips Technical Review*, 1973, **33,** 104–113.
15. Incropera, F. P. and DeWitt, D. P., *Introduction to Heat Transfer*, 3rd edn. Wiley, New York, 1996, p. 118, pp. 124–125, p. 344.
16. Shah, R. K. and London, A. L., *Laminar Flow Forced Convection in Ducts*, Academic Press, New York, 1978, p. 190.
17. Kennedy, D. P., Spreading resistance in cylindrical semiconductor devices. *Journal of Applied Physics*, 1969, **31,** 1490–1497.
18. Busse, C. A., Theory of the ultimate heat transfer limit of cylindrical heat pipes. *International Journal of Heat and Mass Transfer*, 1973, **16,** 169–186.
19. Anderson, D. A., Tannehill, J. C. and Pletcher, R. H., *Computational Fluid Mechanics and Heat Transfer*. Hemisphere, New York, 1984, pp. 549–550.